Osinga, H. M., & Krauskopf, B. (2006). Visualizing curvature on the Lorenz manifold.

Visualizing curvature on the Lorenz manifold

H. M. OSINGA and B. KRAUSKOPF
Engineering Mathematics, University of Bristol, Bristol BS8 1TR, UK

September 2006

Abstract

The Lorenz manifold is an intriguing two-dimensional surface that illustrates chaotic dynamics in the well-known Lorenz system. While it is not possible to find the Lorenz manifold as an explicit analytic solution, we have developed a method for calculating a numerical approximation that builds the surface up as successive geodesic level sets. The resulting mesh approximation can be read as crochet instructions, which means that we are able to generate a three-dimensional model of the Lorenz manifold. We mount the crocheted Lorenz manifold using a stiff rod as the z-axis, and bendable wires at the outer rim and the two solutions that are perpendicular to the z-axis. The crocheted model inspired us to consider the geometrical properties of the Lorenz manifold. Specifically, we introduce a simple method to determine and visualize local curvature of a smooth surface. The colour coding according to curvature reveals a striking pattern of regions of positive and negative curvature on the Lorenz manifold.

1 Introduction

The study of chaotic dynamics is not only an active field of research, but it has lead to quite a number of striking images that are now well known to the general public. Examples are fractal objects [12, 18, 20], such as the Mandelbrot set, and limit sets of Kleinian groups [13], as well as a large number of intriguing chaotic attractors [2, 17, 21, 1]. In the latter category is the 'butterfly attractor' or Lorenz attractor of the famous Lorenz equations [11]. This prototypical chaotic dynamical system is defined as a system of three ordinary differential equations:

$$\begin{cases} \dot{x} &= \sigma(y-x), \\ \dot{y} &= \varrho x - y - xz, \\ \dot{z} &= xy - \beta z. \end{cases} \tag{1}$$

We use the standard values $\sigma = 10$, $\varrho = 28$, and $\beta = \frac{8}{3}$, for which the system has the Lorenz attractor shown in Fig. 1(a). Integrating system (1) from (almost) any initial condition (x_0, y_0, z_0), after disregarding transient effects, will result in an image of this object. An orbit on the Lorenz attractor spirals around one of the 'wings of the butterfly' for some time and then switches, seemingly at random, to the other wing. Note that the system is symmetric under rotation by π about the z-axis, and the attractor also has this symmetry.

This paper deals with a related, yet somewhat complementary object, called the *Lorenz manifold*. It is the two-dimensional smooth surface of all points that converge to the origin $\mathbf{0} = (0, 0, 0)$ of system (1). In other words, points on the Lorenz manifold are special because their orbits do not wander around the Lorenz attractor (as those of practically all other initial conditions do). Locally near $\mathbf{0}$ the Lorenz manifold distinguishes points that move towards the left wing of the attractor from those that

move towards the right wing. Therefore, it 'organises' more globally how points move in (x, y, z)-space under the influence of the Lorenz equations (1). In particular, the Lorenz manifold has the intriguing property that it 'rolls' into the Lorenz attractor without intersecting any orbits on it; see already Fig. 1(b) and Sec. 2 below.

We reveal here some of the aestetic qualities of the Lorenz manifold by considering properties of a crocheted model. This hands-on object is not only a great tool to communicate geometry to specialists and non-specialists alike, but it also lead us to think again about some of the mathematical properties of the Lorenz manifold. We concentrate here on the question how its curvature varies on this two-dimensional surface. Curvature is locally encoded by how mesh points are added and removed during the computation of a mesh representation, which we build up in rings from the origin. We introduce a simple method for determining and visualizing the curvature of (a mesh representation of) a smooth surface, and we use it to colour code the Lorenz manifold.

2 Computing and crocheting the Lorenz manifold

We begin by providing a mathematical characterization of the Lorenz manifold; see, for example, [3, 23] for more background information on dynamical systems theory. As can be checked immediately from (1) the point $\mathbf{0}$ is an equilibrium. Furthermore, its linearization, that is, the matrix

$$\begin{pmatrix} -\sigma & \sigma & 0 \\ \varrho & -1 & 0 \\ 0 & 0 & -\beta \end{pmatrix}$$

has eigenvalues

$$-\beta \quad \text{and} \quad -\frac{1}{2}(\sigma+1) \pm \frac{1}{2}\sqrt{(\sigma+1)^2 + 4\sigma(\varrho-1)}.$$

For the standard parameters, $\mathbf{0}$ has two negative eigenvalues -22.828, -2.667 and one positive eigenvalue 11.828, so that $\mathbf{0}$ is a saddle point with two attracting and two repelling directions. It follows from the stable and unstable manifold theorem that $\mathbf{0}$ has a one-dimensional unstable manifold $W^u(\mathbf{0})$, which is a smooth curve in (x, y, z)-space that is tangent to the one-dimensional unstable linear eigenspace. Similarly, the saddle point $\mathbf{0}$ has a two-dimensional stable manifold $W^s(\mathbf{0})$, which is a smooth surface in (x, y, z)-space that is tangent to the two-dimensional stable linear eigenspace. The Lorenz manifold is mathematically the stable manifold $W^s(\mathbf{0})$. The Lorenz system has two other non-trivial equilibria given by $(\pm\sqrt{\beta(\rho-1)}, \pm\sqrt{\beta(\rho-1)}, \rho-1)$, which are each other's image under the symmetry and are located at the centres of the 'wings' of the Lorenz attractor; see Fig. 1(a). Both these equilibria are saddle points with one attracting and two repelling directions.

Like most dynamical systems, the Lorenz system (1) cannot be solved explicitly. This means that it is not possibly to find $W^u(\mathbf{0})$ and $W^s(\mathbf{0})$ analytically and one must resort to numerical techniques to find accurate approximations. Since $W^u(\mathbf{0})$ is one-dimensional, it is straightforward to find a good approximation of it by numerical integration. Namely, both branches can be approximated by forward integration of an initial condition close to $\mathbf{0}$ on the linear approximation of $W^u(\mathbf{0})$ that is defined by the eigenspace associated with the positive eigenvalue 11.828. The result of such a computation is shown in Fig. 1(a) where the branches of $W^u(\mathbf{0})$ are the two curves that start at the origin $\mathbf{0}$ and accumulate on the Lorenz attractor.

Figure 1(a) also shows a first part of $W^s(\mathbf{0})$, which is a disk that lies approximately in the stable eigenspace spanned by the eigenvectors of the two negative eigenvalues of $\mathbf{0}$. It seems straightforward to generalize the computation of one-dimensional manifolds by integration to the computation of $W^s(\mathbf{0})$ by starting from a selection of points on a circle in the stable eigenspace with small radius and

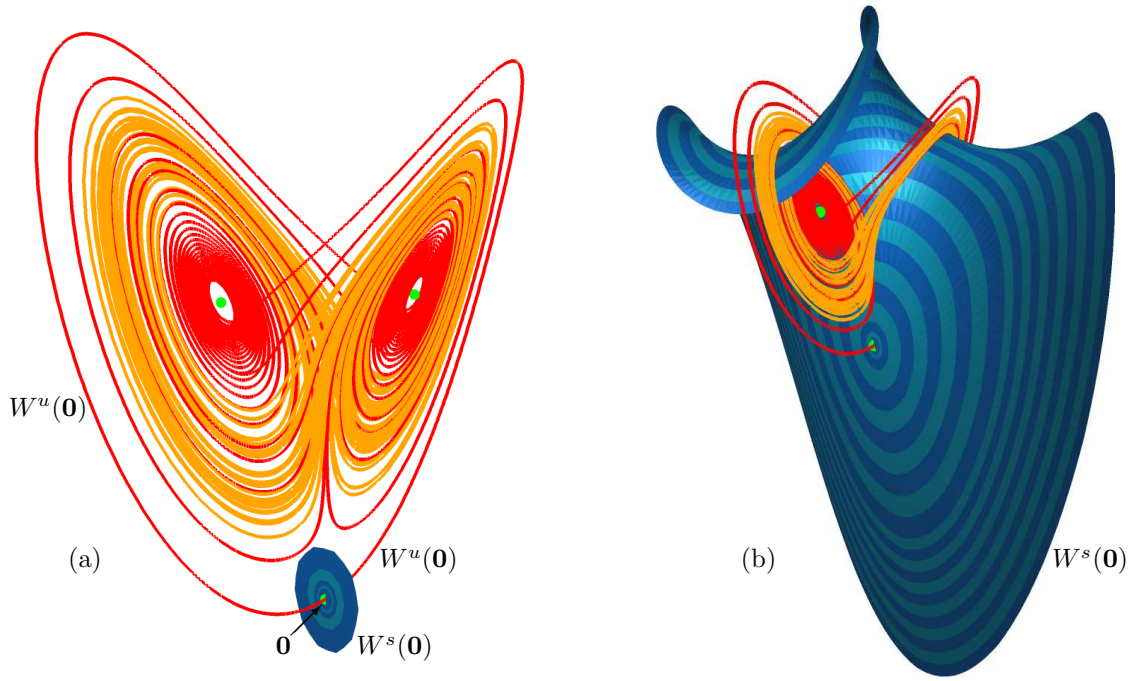

Figure 1: Panel (a) shows how the one-dimensional unstable manifold $W^u(\mathbf{0})$ (red) accumulates on the Lorenz attractor (yellow); also shown is a first almost linear part of the Lorenz manifold $W^s(\mathbf{0})$ (blue). Panel (b) shows how $W^s(\mathbf{0})$ is grown in steps by our method (alternating shades of blue) and rolls into the Lorenz attractor without intersecting it.

centre $\mathbf{0}$. However, it is not at all straightforward how to select suitable (pieces of) orbits on $W^s(\mathbf{0})$ such that an accurate surface can be generated from the data. Due to the very different contraction rates near $\mathbf{0}$, – the ratio of the two eigenvalues -22.828 and -2.667 is about 10 — the dynamics on the manifold causes almost any finite selection of orbits to contain large gaps in resolving the surface; see, for example, [7]. Furthermore, nonlinear effects further away from the origin typically separate orbits quickly. Therefore, specialised algorithms are needed for constructing two-dimensional stable and unstable manifolds, such as the Lorenz manifold $W^s(\mathbf{0})$, as surfaces. In [10] an overview is given of such algorithms, where the Lorenz manifold is used as the example to illustrate how each method works.

Our own method, which is also discussed in [10], is based on the idea of building up the surface by constructing *geodesic level sets*. Recall that the *geodesic distance* between two points is the arclength of the shortest path, called a *geodesic*, on the surface connecting the two points. The geodesic level sets in the present situation are rings of points that have the same geodesic distance to the the origin $\mathbf{0}$, which sits 'in the centre' of the Lorenz manifold $W^s(\mathbf{0})$. As the first ring we take a circle with small radius $\delta > 0$ in the linear eigenspace spanned by eigenvectors of the two corresponding eigenvalues; see Fig. 1(a). We start with a uniformly distributed set of mesh points on this geodesic level set at distance δ. In the next step, a new ring at a slightly larger geodesic distance is constructed point by point using the setup of a two-point boundary value problem. Namely, a point on the new ring is found as the point closest to a given mesh point on the previous ring, with the additional property that it lies on an orbit that passes through the previous ring. Indeed, the previous ring represents the boundary of the two-dimensional surface computed so far. In the case of a stable manifold, all points on this surface converge (approximately) to the equilibrium in forward time. Hence, any point that

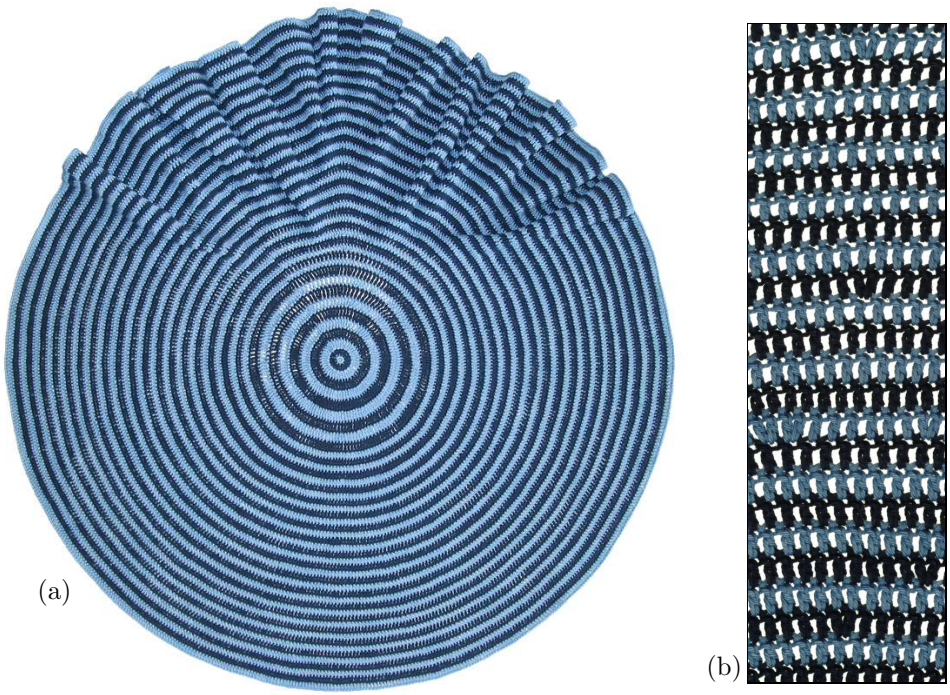

Figure 2: The crocheted Lorenz manifold before mounting (a), and a detail of the crocheted mesh (b).

enters this computed part under forward integration must then also converge to $\mathbf{0}$, which means that it also lies on $W^s(\mathbf{0})$. By repeating this process of adding a new geodesic level set the Lorenz manifold is built up in rings. During the computation new mesh points are added in between consecutive points that lie too far apart, and mesh points are deleted if some points lie too close together. Overall we can ensure that a prescribed mesh quality is maintained so that an accurate mesh representation of the entire surface $W^s(\mathbf{0})$ is calculated. A first part of the Lorenz manifold 'rolling' into the Lorenz attractor is shown in Fig. 1(b). Full details of the algorithm are given in [7, 8], while more computer images of the Lorenz manifold can be found in [9, 14].

Our method of growing the manifold as a collection of geodesic level sets, that is, concentric rings or bands, has the surprising property that it can be interpreted as a crochet instruction; see also [15, 16]. Namely, the distance between corresponding mesh points on two rings is constant for all points on the rings, which means that the same crochet stitch, of a length that respresents this distance, can be used to connect the corresponding mesh points. Where mesh points are added, a two-in-one crochet stitch must be made, while deleted mesh points correspond to decreases in the crocheted work. The resulting crocheted piece is shown in Fig. 2(a) with a detail illustrating the mesh in Fig. 2(b).

As is evident in Fig. 2, the actual three-dimensional positions of the mesh points have not been copied in the crochet instructions. However, the crucial observation is that the pattern of increasing and decreasing crochet stitches is a recipe for encoding the curvature of the manifold locally. The crocheted Lorenz manifold in Fig. 2 is positioned such that the z-axis (which is part of $W^s(\mathbf{0})$) corresponds to a vertical line through the centre point. One can easily observe that the bottom half of the crocheted manifold has very little or no curvature, since this part lies completely flat. On the other hand, it is impossible to make the top half lie flat, as new ripples pop up when others are pressed down. This means that there is a lot of negative curvature in the top half of the Lorenz manifold.

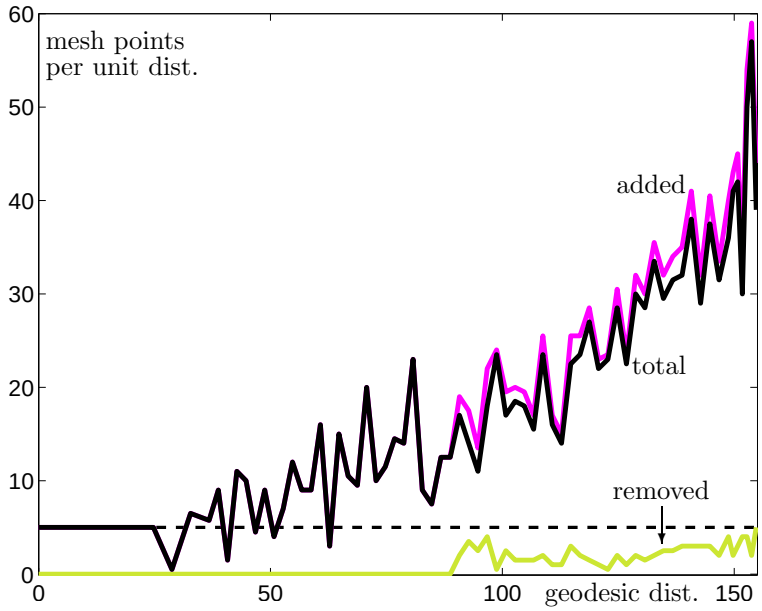

Figure 3: The plot shows how the number of added (magenta), removed (yellow) and total (black) mesh points per unit distance changes during the computation of the Lorenz manifold as a function of geodesic distance. The dashed curve is the constant number of 5 mesh points that would be added per unit distance in the computation of a flat disk.

To get an impression of the overall curvature of the computed Lorenz manifold Fig. 3 shows the added, removed and total (added minus removed) mesh points per unit geodesic distance. The data is up to geodesic distance 155.25; the crocheted models goes up to geodesic distance 110.75. The horizontal dashed line at height 5 corresponds to an object (of the same mesh quality) with zero curvature, that is, a flat disk. A straight line with nonzero positive slope corresponds to a hyperbolic disk, that is, an object with constant negative curvature; indeed, using the same crochet stitch and increasing every kth stitch in each row results in a crocheted model of a hyperbolic disk [4]. The Lorenz manifold is neither a flat disk nor a hyperbolic one. Note that, initially, up to about geodesic distance 25, the total number of mesh points per unit distance is constant. Indeed, this first part of the Lorenz manifold is approximately a flat disk. The overall curvature of the Lorenz manifold is negative, because the total number of mesh points per geodesic level set increases above the horizontal line (from about distance 30 onwards). Furthermore, mesh points are being removed from about distance 90, which indicates regions with positive curvature. Note that the somwhat erratic nature of the graphs in Fig. 3 is a result of the discrete nature of the mesh adaptation during the computation; compare with [8].

As was mentioned, the floppy object in Fig. 2 encodes the true shape of the Lorenz manifold via the variation in local curvature by increases and decreases in the crochet. To bring out its geometrical structure the crocheted piece must be mounted according to the instructions provided in [15]. Figure 4(a1) and (b1) shows the mounted crocheted Lorenz manifold alongside the computed Lorenz manifold as seen from two different view points. A stiff rod was inserted in the location of the z-axis, and bendable wire of the correct length was inserted along the boundary of the computed manifold. To provide some additional support a wire was also inserted along the two orbits on the Lorenz manifold that are perpendicular to the z-axis (which form the so-called strong stable manifold of $\mathbf{0}$). As explained in [15] this is enough to create a good match with the Lorenz manifold as computed.

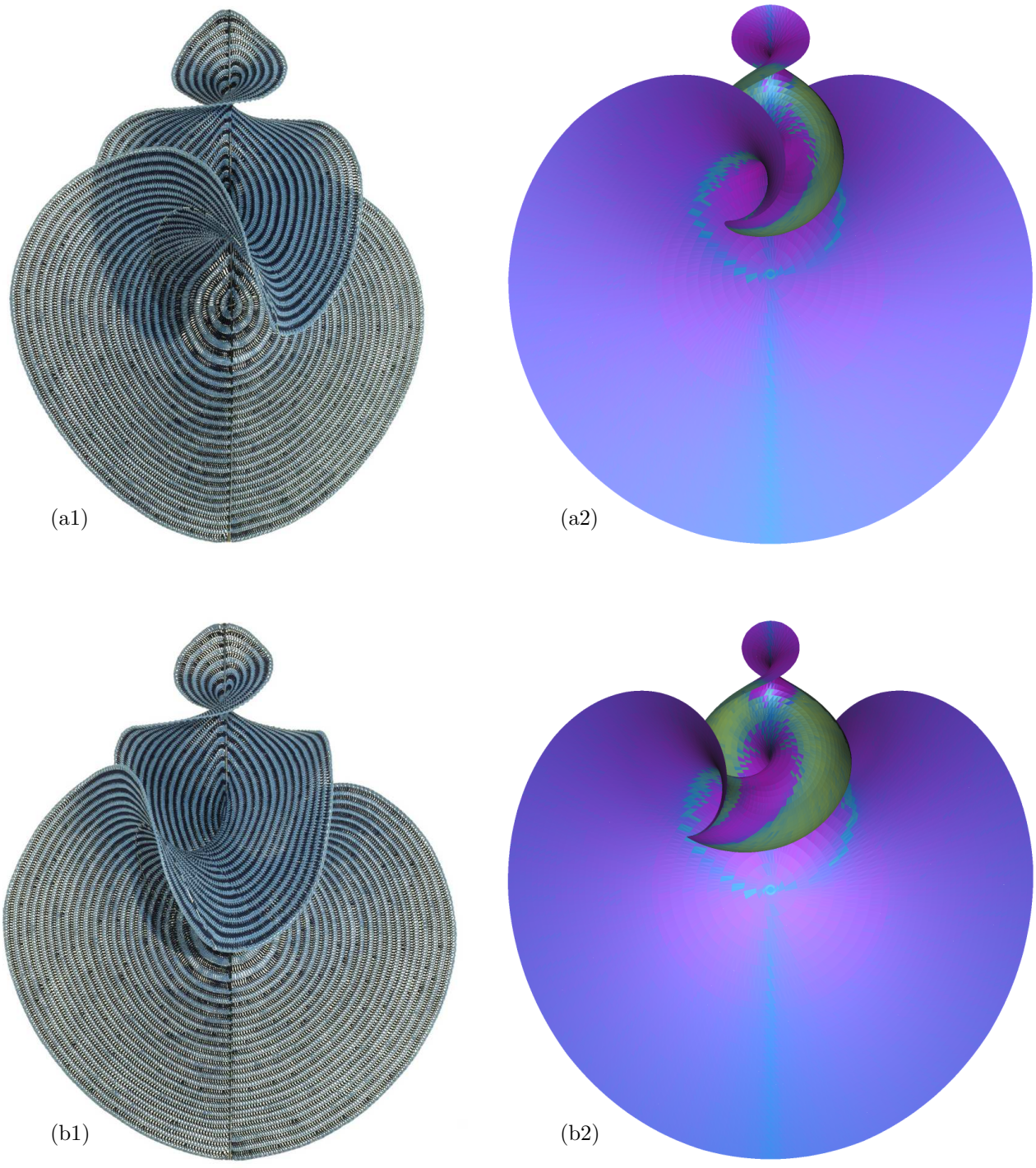

Figure 4: Two views, (a1) and (b1), of the crocheted Lorenz manifold, and the corresponding views, (a2) and (b2), of the computed Lorenz manifold with curvature information. Zero curvature is blue, positive curvature is in shades of green to yellow, and negative curvature is in shades of purple; see also the colour bar in figure 6.

3 Determination and visualization of curvature

Overall, the crocheted model agrees well with the computer generated images. The two views of the crocheted model in Fig. 4(a1) and (b1) are indeed in good agreement with the two corresponding views of the computed Lorenz manifold in Fig. 4(a2) and (b2). However, there are differences and they effectively have to do with the curvature of the Lorenz manifold, which is illustrated in Fig. 4(a2) and (b2) by a colour scheme; see the color bar in Fig. 6. The colour changes from magenta (high negative curvature) via blue (zero curvature) to yellow (high positive curvature). Figure 4 clearly demonstrates that the correspondence between the computer and crocheted representations is worst exactly in those places where the curvature is positive (the yellow regions). In fact, this is a result of the way we mount the crochet model with wires. Generally speaking, any membrane that is stretched by supporting wires will minimize surface tension. This results in a good representation of the actual surface when the curvature is negative or close to zero. On the other hand, areas of positive curvature do not optimize surface tension and may get 'flattened' by the mounting. This is exactly what one notices in Fig. 4, especially near the boundary wire. Indeed, additional wire (or a different kind of support such as starching) would be necessary to create the bulging (yellow) regions on the surface.

The issue of curvature of the Lorenz manifold arose directly from our contemplation of the crocheted model. In order to explain how we obtained the colour representation of the curvature on the surface, we begin by recalling some facts about curvature; see, for example, [22, Chs. 1–3]. We begin with the curvature of a smooth planar curve. At a given point q on the curve, consider the circle through q and two nearby points p_1 and p_2 on either side of q. The limiting circle for $p_1, p_2 \to q$ is called the *osculating circle* at q, and the inverse of its radius is the curvature $k(q)$ at the point q. A point where the curvature is zero the osculating circle is degenerate, namely it coincides with the tangent at q. Note that there is an orientation to the curvature, which is given by whether the curve lies on the left or right of the tangent (with respect to the parametrization of the curve).

If the curve is represented numerically by a mesh of a fixed mesh quality, as expressed by a mesh norm $\|\mathbf{h}\|$, then one can approximate the curvature $k(q)$ at a point q as follows. We first consider the case that the mesh is uniform, meaning that the mesh norm is given by the fixed mesh size $\|\mathbf{h}\| = h$. Take p_1 and p_2 to be the two neighbouring mesh points at distance h from q and let r be the radius of the circle through these three points. Then it follows that $\sin(\alpha) = \|\mathbf{h}\|/(2r)$, where α is the base angle $\angle(q, p_1, p_2) = \angle(q, p_2, p_1)$ of the triangle with corners p_1, q, p_2. The equality $\sin(\alpha) = \|\mathbf{h}\|/(2r)$ is still approximately valid for a nonuniform mesh, where p_1 and p_2 are at slightly different distances of approximately $\|\mathbf{h}\|$ from q; compare with [5, 6].

Since $1/r = 2\sin(\alpha)/\|\mathbf{h}\|$ is an approximation of the curvature $k(q)$, we define the *one-dimensional curvature indicator*

$$c_I(q) := \frac{2\,(p_1 - q)\cdot \mathbf{n}}{\|\mathbf{h}\|^2}\,,$$

where $\mathbf{n}$ is the normal of the approximate tangent $p_1 - p_2$ at q. Note that, by construction of the normal $\mathbf{n}$, we have that $(p_1 - q)\cdot\mathbf{n} = (p_2 - q)\cdot\mathbf{n}$, so that $c_I(q)$ is independent of the choice of neighbour used in its definition. Furthermore, the curvature indicator $c_I(q)$ converges to the curvature $k(q)$ as the mesh norm $\|\mathbf{h}\|$ goes to zero.

If we now consider the two-dimensional curvature at a point q on a surface in three-dimensional space, it seems natural to consider the curvatures of the intersection curves that are obtained by intersecting the surface with arbitrary planes through q. Already in 1760, Euler considered all planes spanned by the normal of the surface at q and an arbitrary tangent vector v_i at q. He found that, if the associated curvatures are not all equal, then there is precisely one direction, say v_1, for which the curvature takes a minimal value, and precisely one direction, say v_2, in which it takes a maximum

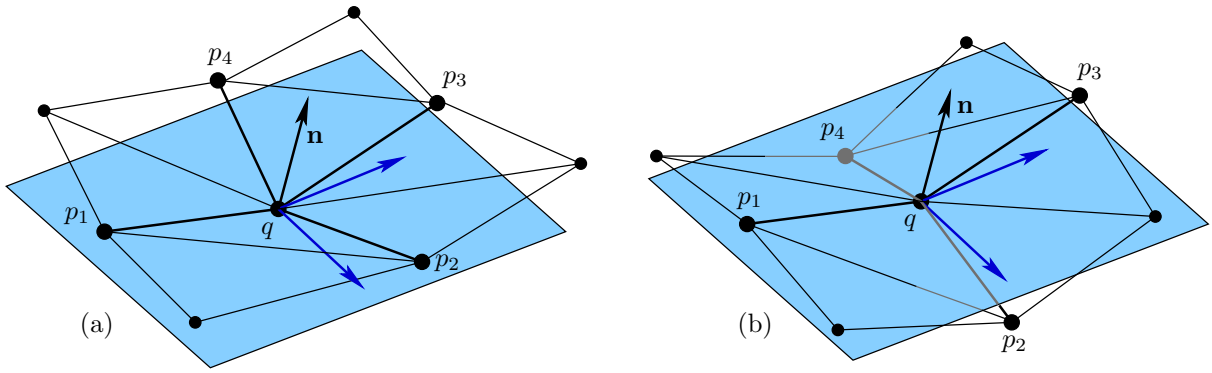

Figure 5: The curvature indicator (3) at the point q is determined from its direct neighbours p_1 to p_4 of the mesh by considering the normal $\mathbf{n}$ of the approximate tangent plane at q spanned by $p_3 - p_1$ and $p_4 - p_2$. In the case of positive curvature (a) the points p_1 to p_4 all lie on the same side of the plane $\mathcal{S}$, while in the case of positive curvature (b) this is not the case.

value. In fact, these two directions are perpendicular. Gauss formulated these findings and developed the ideas further in 1827. He defines the curvature of the surface at the point q as the product of the minimum and maximum curvature. If the product and, hence, the curvature at q is positive then the entire surface curves away from the tangent plane at q in the same direction. Thus, the surface is locally convex near a point q where the curvature is positive. On the other hand, if the product and, hence, the curvature at q is negative then the surface is locally a saddle near q.

Our goal is to provide a fast and convenient way of determining and visualizing how curved a given surface actually is. We assume that the surface is represented by a mesh representation (typically a triangulation) of a quality given by the mesh norm $\| \mathbf{h} \|$. In this situation one can only expect to obtain an estimate of the curvature at a given mesh point q. In particular, we want to avoid solving the optimization problem of finding (approximate) directions of minimal and maximal curvature. Consider the four neighbours p_1, p_2, p_3 and p_4 of the point q (at approximately distance $\| \mathbf{h} \|$ from q) as shown in Fig. 5. We assume here that the points p_1 to p_4 are labelled such that the two curve approximations $\overline{p_1 q p_3}$ and $\overline{p_2 q p_4}$ intersect each other transversely at q. The idea is now to use the (approximate) one-dimensional curvature indicators of $\overline{p_1 q p_3}$ and $\overline{p_2 q p_4}$. We consider the normal $\mathbf{n}$ of the approximate tangent plane at q given by the normalized cross product

$$\mathbf{n} = \frac{(p_3 - p_1) \times (p_4 - p_2)}{\| (p_3 - p_1) \times (p_4 - p_2) \|} ,$$

and define the numbers

$$\kappa_i = \frac{2\,(p_i - q) \cdot \mathbf{n}}{\| \mathbf{h} \|^2} . \tag{2}$$

Note that κ_1 and κ_2 are only approximations of the one-dimensional curvature indicators of the intersection curves of the surface with the planes spanned by p_1, q, p_3 and by p_2, q, p_4, respectively, because the normal $\mathbf{n}$ does not generally lie in either of these planes. Furthermore, by construction of the approximate tangent plane, we have that $\kappa_1 = \kappa_3$ and $\kappa_2 = \kappa_4$.

The *two-dimensional curvature indicator* $C_I(q)$ is then defined as

$$C_I(q) = \kappa_1 \kappa_2 . \tag{3}$$

Again, $C_I(q)$ is independent of the choice of neighbours used in its definition.

The situations for both positive and negative curvature near q are illustrated in Fig. 5. Note that $C_I(q)$ correctly identifies (within the limits of the mesh representation) whether the curvature is positive or negative, since it effectively compares the location of the neighbouring points with the (approximate) tangent plane. Furthermore, the larger $|C_I(q)|$ the more curved the surface is. Therefore, $C_I(q)$ is indeed a good indicator of curvature while being cheap and fast to compute. On the other hand, $C_I(q)$ is not designed to give the actual value of curvature at q. This is because we do not attempt to find the directions of minimal and maximal curvature.

Colour coding the Lorenz manifold in terms of its curvature is indeed a very valuable tool, as was already clear from Fig. 4(a2) and (b2). Specifically for stable or unstable manifolds computed using our method [7, 8] of constructing geodesic level sets, the mesh is very nice and uniform. In particular, the mesh is constructed such that $\overline{p_1 q p_3}$ and $\overline{p_2 q p_4}$ are approximately perpendicular. What is more, the mesh is such that the neighbours p_1 to p_4 of q have special meaning. Namely, two neighbouring mesh points (say, p_1 and p_3) are on a geodesic level set, and the other two neighbouring mesh points (say, p_2 and p_4) lie on consecutive rings, that is, on an approximate geodesic. Therefore, one term in the definition on $C_I(q)$ is an approximation of the geodesic curvature [22] in our case. We remark that geodesic curvature is used in our algorithm to determine the distance between consecutive computed rings; see [8] for details.

Figure 6 shows the Lorenz manifold computed up to the geodesic level set of distance 155.25 and colour coded with a scaled version of the two-dimensional curvature indicator. Namely, for a fixed mesh of norm $\|\mathbf{h}\|$ it suffices to compute

$$[(p_1 - q) \cdot \mathbf{n}]\,[(p_2 - q) \cdot \mathbf{n}]$$

for each mesh point q. The resulting range of positive and negative values are translated into a colour coding according to the colour bar in Fig. 6. To obtain a better colour distribution on the Lorenz manifold, we used a nonlinear scaling by taking the square root. The result was visualized with the package GEOMVIEW [19]; see also [14] for more details.

As Fig. 6(a) shows, the helical structure along the positive z-axis is associated with large negative curvature. However, because the Lorenz manifold also rolls up into the Lorenz attracor, two scrolls are generated. The transition region between the helix and the scrolls is associated with bands of positive curvature; see the enlargement in Fig. 6(b). It is known that the helix along the z-axis is periodic in the limit of large z. As one observes in Fig. 6(a) and (b), this leads to an almost periodic curvature pattern. The further enlargement in Fig. 6(c) shows a secondary helix, which follows the helix about the z-axis. Its curvature pattern is very similar to that of the main helix. As was noted in [14], there are infinitely many (symmetrically related) pairs of such secondary helices.

4 Conclusions

We discussed the curvature properties of the Lorenz manifold by means of a two-dimensional curvature indicator that is fast and simple to calculate for a given mesh representation. The indicator is based on neighbouring mesh points of a given point and involves only cross and dot products of vectors. Our method of building up the Lorenz manifold by geodesic level sets generates a regular and well-spaced mesh that is well suited for calculating the curvature indicator. The information was translated into a colour code, which brought out contrasting regions of positive and negative curvature.

The curvature indicator is not specific to the Lorenz manifold, nor to the way we computed a mesh representation. Rather, it can be used to bring to light the geometry of any complicated surface represented by a regular mesh. By adjusting the colour code, geometric features may be highlighted and striking images created.

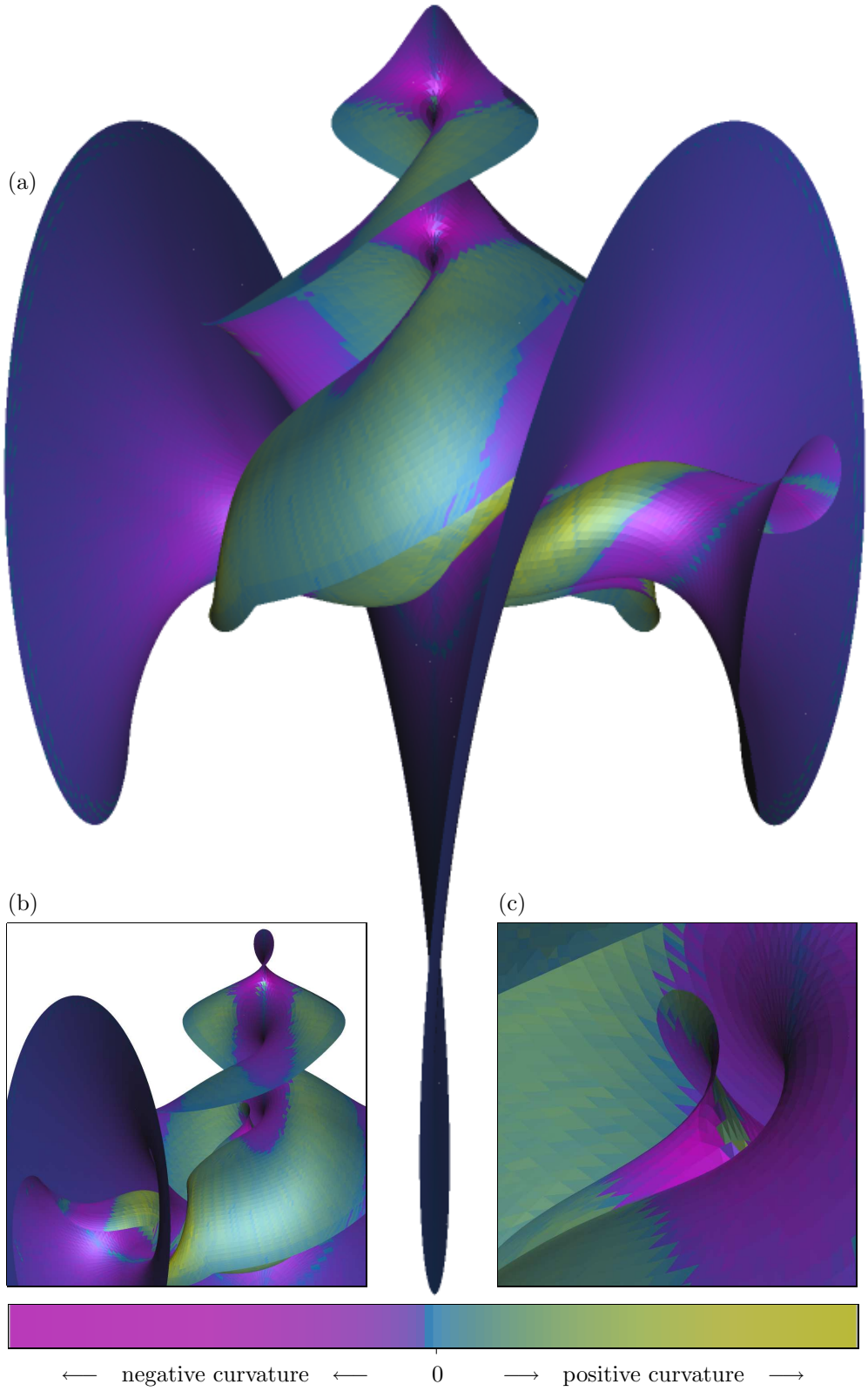

Figure 6: The Lorenz manifold computed up to geodesic distance 155.25 with curvature information (a), an enlarged different view (b), and an further enlargement near a secondary helix (c). Curvature is visualized as given by the colour bar.

Acknowledgements

We thank Benjamin Storch for interesting discussions and for pointing out the possibility of positive curvature on the crocheted Lorenz manifold. Both authors are supported by EPSRC Advanced Research Fellowships.

References

[1] Chapman, R. S. and Sprott, J. C., 2005, *Images of a Complex World: The Art And Poetry of Chaos* (Singapore: World Scientific).

[2] Field, M. and Golubitsky, M., 1995, *Symmetry in Chaos, A search for pattern in mathematics, art and nature* (Oxford, UK: Oxford University Press), (Corrected reprint of the 1992 original).

[3] Guckenheimer, J. and Holmes, P., 1983 *Nonlinear Oscillations, Dynamical Systems, and Bifurcations of Vector Fields*, Applied Mathematical Sciences **42** (New York: Springer-Verlag).

[4] Henderson, D.W. and Taimina, D., 2001, Crocheting the hyperbolic plane. *The Mathematical Intelligencer,* **23**(2), 17–28.

[5] Hobson, D., 1993, An efficient method for computing invariant manifolds of planar maps. *Journal of Computational Physics* **104**(1), 14–22.

[6] Krauskopf, B. and Osinga, H. M., 1999, Growing 1D and quasi 2D unstable manifolds of maps. *Journal of Computational Physics* **146**(1), 404–419.

[7] Krauskopf, B. and Osinga, H. M., 1999, Two-dimensional global manifolds of vector fields. *CHAOS,* **9**(3), 768–774.

[8] Krauskopf, B. and Osinga, H. M., 2003, Computing geodesic level sets on global (un)stable manifolds of vector fields. *SIAM Journal on Applied Dynamical Systems,* **2**(4), 546–569.

[9] Krauskopf, B. and Osinga, H. M., 2004, The Lorenz manifold as a collection of geodesic level sets *Nonlinearity,* **17**(1), C1–C6.

[10] Krauskopf, B., Osinga, H. M., Doedel, E. J., Henderson, M. E., Guckenheimer, J., Vladimirsky, A., Dellnitz, M. and Junge, O., 2005, A survey of methods for computing (un)stable manifolds of vector fields. *International Journal of Bifurcation and Chaos,* **15**(3), 763-791.

[11] Lorenz, E. N., 1963, Deterministic nonperiodic flows. *Journal of the Atmospheric Sciences,* **20**, 130–141.

[12] Mandelbrot, B. B., 1982, *The Fractal Geometry of Nature* (New York: W. H. Freeman and Co.)

[13] Mumford, D., Series, C. and Wright, D., 2002, *Indra's Pearls, The vision of Felix Klein* (New York: Cambridge University Press).

[14] Osinga, H. M. and Krauskopf, B., 2002, Visualizing the structure of chaos in the Lorenz system. *Computers and Graphics,* **26**(5), 815–823.

[15] Osinga, H. M. and Krauskopf, B., 2004, Crocheting the Lorenz manifold. *The Mathematical Intelligencer,* **26**(4), 25–37; see also `http://www.enm.bris.ac.uk/staff/hinke/crochet/`

[16] Osinga, H. M. and Krauskopf, B., 2006, The Lorenz manifold: Crochet and Curvature. In: R. Sarhangi and J. Sharp (Eds) Proceedings of *Bridges London: Mathematical Connections in Art, Music, and Science*, London, UK, 4-9 August (St Albans, UK: Tarquin Publications), pp. 255–260.

[17] Ott, E., 2002, *Chaos in Dynamical Systems* (New York: Cambridge University Press), second edition.

[18] Peitgen, H.-O., Jürgens, H. and Saupe, D., 1992, *Chaos and Fractals: New Frontiers of Science* (New York: Springer-Verlag).

[19] Phillips, M., Levy, S. and Munzner, T., 1993, Geomview: An interactive geometry viewer. *Notices of the American Mathematical Society* **40**, 985–988.

[20] Pickover, C. A., 1995, *The Pattern Book: Fractals, Art, and Nature* (Singapore: World Scientific).

[21] Rabinovich, M. I., Ezersky, A. B. and Weidman, P. D., 2000 *The Dynamics of Patterns* (Singapore: World Scientific).

[22] Spivak, M., 1975, 1979, *A Comprehensive Introduction to Differential Geometry*, Volume 2 (Houston, TX: Publish or Perish, Inc.), second edition.

[23] Strogatz, S., *Nonlinear Dynamics and Chaos* (Boston, MA: Addison Wesley).